scientific reports

OPEN

Hall current effect in bioconvection Oldroyd-B nanofluid flow through a porous medium with Cattaneo-Christov heat and mass flux theory

Noor Saeed Khan[1], Somchai Sriyab[2]✉, Attapol Kaewkhao[2] & Ekkachai Thawinan[2]

Bioconvection due to microorganisms is important area of research, considerably importance for environment and sustainable fuel cell technologies. Buongiorno nanofluid model for Cattaneo-Christov heat and mass flux theory taken into account the Oldroyd-B nanofluid and gyrotactic microorganisms in a rotating system with the effects of Hall current, and Darcy porous medium is scrutinized. The constitutive equations of the problem are transformed into nondimensional equations with the help of similarity transformations. Homotopy analysis method is used to obtain the solution. Graphs and table support the comprehesive representation of the achieved results. Radial velocity is reduced with the increasing values of relaxation time, retardation time and magnetic field parameters while heat transfer is augmented with thermal relaxation time parameter. The nanoparticles concentration is reduced with the increasing values of Schmidt number and the gyrotactic microorganisms concentration is enhanced with the increasing values of Peclet number. A nice agreement is obtained while comparing the present results numerically with the published results. The proposed mathematical model is used in biochemical engineering, meteorology, power and transportation production, optoelectronic and sensing microfabrication.

Heat transfer performance is enhanced on account of adding the micro size particles in the base liquids. The improved heating conduction of nanofluids has shown better results. Nanofluids are used in cooling of metalic plates, paper productions, drawing of plastic sheets, aerodynamics, etc. When the nanofluids are regulated by magnetic field, then these have potential applications such as anticancer drugs with the magnetic nanoparticles. Considering the applied magnetic field, Mandal and Pal[1] analyzed the carbon nanotubes nanofluid with homogeneous-heterogeneous chemical reactions, variant heating transportation and mass diffusion, binary chemical reaction and activation energy using the convective boundary conditions. Yaseen et al.[2] worked on the magnetohydrodynamic hybrid and mono nanoliquids within two shrinking and revolving discs through a Darcy-Forchheimer permeable medium considering Cattaneo-Christov (C-C) heat flux theory, viscous dissipation, Ohmic heating, solar radiation and heating generating/absorbing phenomena. Mandal[3] used the fifth order Runge-Kutta-Fehlberg method in the presence of shooting procedure to solve the problem of convection boundary layer flow and heat transfer of micropolar nanofluid containing four types of nanoparticles on a nonlinear expanding source. Garia et al.[4] scrutinized the magnetohydrodynamic motion of water based hybrid suspension on two surfaces by implementing the Das and Tiwari concept by considering the C-C heating transportation theory. They computed the coefficients of correlation of heating transportation and skin friction processed by the evaluation of probable error and statistical declaration. Pal and Mandal[5] obtained the dual solutions of mixed convection-radiation stagnation point motion of three nanofluids through a porous medium over an expanding/contracting space by using the Runge-Kutta-Fehlberg procedure in connection to shooting algorithm which shows that the size of boundary layer is high for second solution compared to that of first solution. Rawat and Kumar[6] worked on the water based copper nanofluid stagnation point flow with C-C concept and heating generating/absorbing phenomena, thermal radiation, activation energy, suction and slip condition which proved

[1]Department of Mathematics, Division of Science and Technology, University of Education, Lahore 54000, Pakistan. [2]Research Group in Mathematics and Applied Mathematics, Department of Mathematics, Faculty of Science, Chiang Mai University, Chiang Mai 50200, Thailand. ✉email: somchai.sriyab@gmail.com

that thermal relaxation and radiation parameters enhance the heat transfer while slip and suction parameters reduce the mass transfer. Some nanofluids literature can be read from the references[7–16].

Recently, non-Newtonian liquids have gained a wide range of importance in manufacturings, commerce and mechanics which are seen in food processsing, material handling, oil storage, warehousing etc. In general, non-Newtonian suspensions possess three leading classifications as differential, rate and integral types in which the rate type shows the stress relaxation. Oldroyd-B class holds the rate-type fluid which possess the generalization of the upper convected viscoelastic Maxwell fluid class in the possession of retardation time and presents the motion of viscoelastic fluids propposed by Oldroyd[17]. Hafeez et al.[18] looked over the Oldroyd-B fluid in the existence of C-C heating transportation theory, homogeneous-heterogeneous reactions by using the BVP Midrich technique in which the flow speed becomes slow due to the effect of relaxation time factor. Shahzad et al.[19] worked on the Das and Tiwari nanoliquid concept to investigate the thermal characteristics of Oldroyd-B fluid with engine oil as a conventional base suspension. They proved that the heating conduction of molybdenum disulfide engine oil nanofluid is greater than the copper engine oil nanofluid. Irfan et al.[20] performed the analysis of double stratification in nonlinear radiative flow of Oldroyd-B nanofluid in stagnation region with the effects of magnetohydrodynamic and heat source/sink, Brownian diffusion and thermophoresis. Anwar et al.[21] explained the transient free convection motion of an Oldroyd-B liquid through a vertical porous channel with nonlinear solar radiation in which the one side flow direction has unsteady velocity, while other side performs no movement on the basis of momentum conservation law and Fourier's principle of heat transfer. Irfan et al.[22] used the convective conditions in chemically reactive radiated Oldroyd-B nanofluid with buoyancy, magnetic and Joule heating effects. The different chrateristics of Oldroyd-B nanofluid are investigated by Irfan et al.[24–26]. Khan et al.[23] investigated the Oldroyd-B liquid taken into account the C-C heat and mass flux theory using Darcy-Forchheimer effect to probe the bioconvection heating and nanoparticles concentration retaining gyrotactic microbs through a permeable source. Hafeez et al.[27] worked on the modelling of heating transportation and nanoparticles concentration in the dynamics of Oldroyd-B nano-suspension with C-C heat and mass flux theory taken into account the Buongiorno nanofluid formulation. Usman et al.[28] focused on the behavior associated with Oldroyd-B nanofluid thin film sprinkled on an extended cylinder accommodating nanoparticles and gyrotactic microorganisms with heat transfer by implementing the Homotopy Analysis Method (HAM). Khan et al.[29] considered the Oldroyd-B fluid configured by infinite stretching disks with slip effects and homogeneous-heterogeneous chemical reactions. Hashmi et al.[30] formulated a problem discussing the heat source/sink, viscous dissipation and Joule heating in mixed convection axisymmetric flow of an incompressible, electrically conducted Oldroyd-B fluid in two infinite isothermal stretching disks. Tong et al.[31] presented the thermal behaviors of bioconvection Oldroyd-B nanofluid in the light of slip, thermal radiation, activation energy, magnetic force and porous medium effects with Cattaneo-Christov heat and mass flux theory. Hashmi et al.[32] considered the steady heating and mass transferring motion of Oldroyd-B fluid with isothermal/exothermic reaction incarporating the features of Ohmic dissipation and Joule heating. The non-Newtonian features and others properties of various suspensions are exist in the studies[33–38].

Bioconvection takes place in the suspension on account of up-swimming microorganisms which leads to the unstable density stratification, shows considerably importance for environment and sustainable fuel cell technologies having uses in environmental systems like ocean algae, fuel cells and biological polymer synthesis. The addition of nanofluid and bioconvection has obtained very important achievements in micro-fluidic devices including micro-reactors and micro-channel. Waqas et al.[39] addressed the bioconvection effect due to microorganisms in Jeffery nanofluid past an expanding surface by considering the magnetic dipole effect. Raja et al.[40] applied the soft computing based backpropagated neural networks with Levenberg marquardt technique to a bioconvection second-grade nanofluid model with C-C heat and mass flux theory, Hall current effect and porous medium. Waqas et al.[41] discussed the numerical study of Oldroyd-B nanofluid flow with heat and mass transfer, gyrotactic microorganisms past a rotating disk through bvp4c built-in function of MATLAB software. Khan et al.[42] analyzed the bioconvection nano-suspension motion and entropy generation in rotating system with the application of Homotopy Analysis Method. Rashad and Nabwey[43] described the bioconvection of a nanofluid pertaining to motile microorganisms over a horizontal circular cylinder under the convective boundary conditions using Buongiorno's nanofluid model with the Oberbeck-Boussinesq approximation. Alwatban et al.[44] analyzed the bioconvection in magnetic nanoparticles using Wu's slip effects near the surface. Lv et al.[45] introduced a new form of non-Newtonian liquid called Reiner-Rivlin nanofluid past a rotating disk with C-C heat flux through a porous media in the presence of gyrotactic microorganisms. Shehzad et al.[46] studied the bioconvection flow of Maxwell fluid past the isolated disk by considering the Buongiorno nanofluid model with Cattaneo-Christov energy and mass species flux models. Related studies are mentioned in the references[47–51].

The aforementioned literature contains different aspects associated with different fluids and are interesting studies. Strong applied magnetic field with permeable media associated to gyrotactic microorganisms along a revolving disk in the presence of Oldroyd-B nano-suspension needs attention to be investigated. So the authors studied the Oldroyd-B nano-suspension motion over an expandable revolving disc in the light of C-C model soved through[52].

Procedure

Problem formulation. The swirl of Oldroyd-B nanofluid retaining gyrotactic microorganisms in porous space for three dimensions is modelled. Heat and mass transfer modeling is obtained through C-C concept. For Hall current effect, strong magnetic field is in implementation to perpendicular side (consider the Fig. 1).

Considered problem has the dynamic mechanisms[18,27,28,42].

$$\frac{\partial u}{\partial r} + \frac{u}{r} + \frac{\partial w}{\partial z} = 0, \tag{1}$$

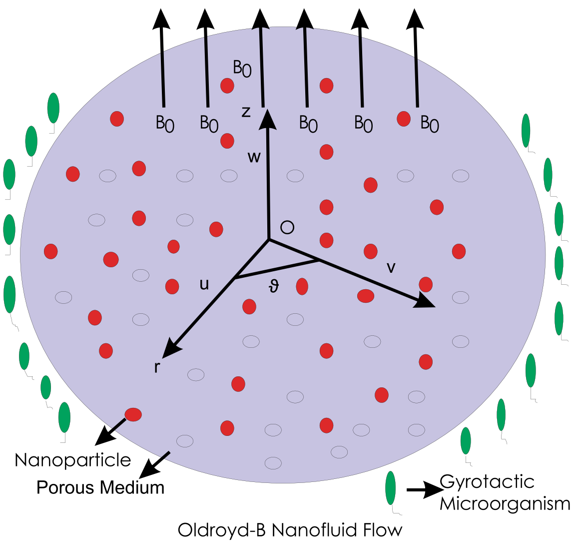

Figure 1. A plot presents the modeling.

$$
\begin{aligned}
&\rho_f \left(u\frac{\partial u}{\partial r} + w\frac{\partial u}{\partial z} - \frac{v^2}{r}\right) \\
&= \mu_f \frac{\partial^2 u}{\partial z^2} + \lambda_1 \left(\frac{uv^2}{r^2} + \frac{u^2\partial^2 u}{\partial r^2} + w^2\frac{\partial^2 u}{\partial z^2} + 2uw\frac{\partial^2 u}{\partial r \partial z} - \frac{2}{r}uv\frac{\partial v}{\partial r} - \frac{2}{r}vw\frac{\partial v}{\partial z} + \frac{1}{r^2}uv^2 + \frac{1}{r}v^2\frac{\partial u}{\partial r}\right) \\
&- \lambda_2\mu_f \left[-\frac{1}{r}\left(\frac{\partial u}{\partial z}\right)^2 - 2\frac{\partial u}{\partial z}\frac{\partial^2 w}{\partial z^2} + w\frac{\partial^3 u}{\partial z^3} - \frac{\partial u}{\partial r}\frac{\partial^2 u}{\partial z^2} - \frac{\partial u}{\partial z}\frac{\partial^2 u}{\partial r\partial z} + u\frac{\partial^3 u}{\partial r \partial z^2}\right] \\
&- \frac{\sigma_f B_0^2 (u - mv + w\lambda_1\frac{\partial u}{\partial z})}{1+m^2} \\
&- \frac{\mu_f}{k}u - k^F u^2,
\end{aligned} \tag{2}
$$

$$
\begin{aligned}
&\rho_f \left(u\frac{\partial v}{\partial r} + w\frac{\partial v}{\partial z} + \frac{1}{r}uv\right) \\
&= -\lambda_1 \left(-\frac{2vu^2}{r^2} + \frac{u^2\partial^2 v}{\partial r^2} + w^2\frac{\partial^2 v}{\partial z^2} + 2uw\frac{\partial^2 v}{\partial r\partial z} + \frac{2}{r}uv\frac{\partial u}{\partial r} + \frac{2}{r}vw\frac{\partial u}{\partial z} - \frac{2}{r^2}vu^2 - \frac{1}{r^2}v^3 + \frac{1}{r}v^2\frac{\partial v}{\partial r}\right) \\
&+ \mu_f\frac{\partial^2 v}{\partial z^2} + \lambda_2\mu_f \left[-\frac{u}{r}\frac{\partial^2 v}{\partial z^2} + w\frac{\partial^3 v}{\partial z^3} - 2\frac{\partial v}{\partial z}\frac{\partial^2 w}{\partial z^2} - \frac{1}{r}\frac{\partial v}{\partial z}\frac{\partial u}{\partial z} + \frac{v}{r}\frac{\partial^2 u}{\partial z^2} - \frac{\partial^2 u}{\partial z^2}\frac{\partial v}{\partial r} - \frac{\partial v}{\partial z}\frac{\partial^2 u}{\partial r\partial z} - \frac{u}{r}\frac{\partial^2 v}{\partial z^2}\right] \\
&- \frac{\sigma_f B_0^2 (v + mu + w\lambda_1\frac{\partial v}{\partial z})}{1+m^2} \\
&- \frac{\mu_f}{k}w - k^F w^2,
\end{aligned} \tag{3}
$$

$$
\begin{aligned}
&\left(u\frac{\partial T}{\partial r} + w\frac{\partial T}{\partial z}\right) \\
&= \alpha\frac{\partial^2 T}{\partial z^2} + 2\gamma_1\tau\frac{D_T}{T_\infty}\left[u\frac{\partial T}{\partial z}\frac{\partial^2 T}{\partial r\partial z} + w\frac{\partial T}{\partial z}\frac{\partial^2 T}{\partial z^2}\right] + \tau\left[D_B\left(\frac{\partial T}{\partial z}\frac{\partial C}{\partial z}\right) + \frac{D_T}{T_\infty}\left(\frac{\partial T}{\partial z}\right)^2\right] \\
&+ \gamma_1\tau D_B\left[u\frac{\partial T}{\partial z}\frac{\partial^2 C}{\partial r\partial z} + u\frac{\partial C}{\partial z}\frac{\partial^2 T}{\partial r\partial z} + w\frac{\partial T}{\partial z}\frac{\partial^2 C}{\partial z^2} + w\frac{\partial C}{\partial z}\frac{\partial^2 T}{\partial z^2}\right] \\
&+ \gamma_1\left[u\frac{\partial w}{\partial r}\frac{\partial T}{\partial z} + u\frac{\partial u}{\partial r}\frac{\partial T}{\partial r} + w\frac{\partial u}{\partial z}\frac{\partial T}{\partial r} + w\frac{\partial w}{\partial z}\frac{\partial T}{\partial z} + u^2\frac{\partial^2 T}{\partial r^2} + w^2\frac{\partial^2 T}{\partial z^2} + 2uw\frac{\partial^2 T}{\partial r\partial z}\right],
\end{aligned} \tag{4}
$$

$$
\begin{aligned}
&u\frac{\partial C}{\partial r} + w\frac{\partial C}{\partial z} \\
&= D_B\frac{\partial^2 C}{\partial z^2} + \gamma_2\tau\frac{D_T}{T_\infty}\left[u\frac{\partial^3 T}{\partial r\partial z^2} + w\frac{\partial^3 T}{\partial z^3}\right] + \frac{D_T}{T_\infty}\frac{\partial^2 T}{\partial z^2} \\
&- \gamma_2\left[u\frac{\partial w}{\partial r}\frac{\partial C}{\partial z} + u\frac{\partial u}{\partial r}\frac{\partial C}{\partial r} + w\frac{\partial u}{\partial z}\frac{\partial C}{\partial r} + w\frac{\partial w}{\partial z}\frac{\partial C}{\partial z} + u^2\frac{\partial^2 C}{\partial r^2} + w^2\frac{\partial^2 C}{\partial z^2} + 2uw\frac{\partial^2 C}{\partial r\partial z}\right],
\end{aligned} \tag{5}
$$

$$u\frac{\partial N}{\partial r}+w\frac{\partial N}{\partial z}+\frac{bW_c}{(C_w-C_\infty)}\frac{\partial}{\partial z}\left(N\frac{\partial C}{\partial z}\right)=D_n\left[\frac{\partial^2 N}{\partial r^2}+\frac{1}{r}\frac{\partial N}{\partial r}+\frac{\partial^2 N}{\partial z^2}\right],\tag{6}$$

using B.C. (boundary conditions)

$$u=ra,\ v=r\Omega,\ w=0,\ T=T_w,\ C=C_w,\ N=N_w\ at\ z=0,\tag{7}$$

$$u\to 0,\ v\to 0,\ T\to T_\infty,\ C\to C_\infty,\ N\to N_\infty\ as\ z\to\infty,\tag{8}$$

$u(r,\vartheta,z)$, $v(r,\vartheta,z)$ and $w(r,\vartheta,z)$ have been designed for flow constitutients, P stands for pressure, magnetic field is presented by $B=(0,0,B_0)$, the Hall parameter is m[42]. λ_1, λ_2 show the relaxation and retardation time parameters respectively. Similarly, γ_1 and γ_2 present thermal relaxation and mass relaxation time parameters respectively. Thermal diffusivity is α, permeability of porous medium is k, Forchheimer resistance parameter is $k^F=\frac{C_b}{\sqrt{k}}$, C_b is the drag coefficient, Brownian diffusion coefficient is D_B, thermophoretic diffusion coefficient is D_T, ρ_f exhibits the density, μ_f manifests the dynamic viscosity, σ_f enlightens the electrical conductivity and $(c_p)_f$ represents heat capacity associated with Oldroyd-B nano-suspension. $\nu_f=\frac{\mu_f}{\rho_f}$ exhibits the kinematic viscousity, $\tau=\frac{(\rho c)_P}{(\rho c)_f}$ shows the quantity due to heat capacity, b employs the chemotaxis constant, W_c exhibits the highest cell swimming speed and D_n is the diffusivity of microorganisms.

The following transformations[18,27,46] are introduced

$$\begin{aligned}&u=r\Omega f(\zeta),\ v=r\Omega g(\zeta),\ w=(\Omega\nu_f)^{\frac{1}{2}}h(\zeta),\ \theta(\zeta)=\frac{T-T_\infty}{T_w-T_\infty},\ \phi(\zeta)=\frac{C-C_\infty}{C_w-C_\infty},\\&\chi(\zeta)=\frac{N-N_\infty}{N_w-N_\infty},\ \zeta=\left[\frac{\Omega}{\nu_f}\right]^{\frac{1}{2}}z.\end{aligned}\tag{9}$$

Substituting the values from Eq. (9) in Eqs. (1–8), the below eight equations (10–17) are obtained.

$$2f+h'=0,\tag{10}$$

$$\begin{aligned}&f^2-g^2+f'h-f''+\beta_1\left(h^2f''+2ff'h-2gg'h\right)+\beta_2\left(2f'^2+2f'h''-f'''h\right)\\&-\frac{M(f'-mg-2\beta_1 hf')}{1+m^2}\\&-\lambda_3 f-\lambda_4 f^2=0,\end{aligned}\tag{11}$$

$$\begin{aligned}&2fg+g'h-g''+\beta_1\left(h^2g''+2\left(fg'+gf'\right)h\right)-\beta_2\left(hg'''-2f'g'-2h''g'\right)\\&-\frac{M(mf'+g-2\beta_1 hg')}{1+m^2}\\&-\lambda_3 g-\lambda_4 g^2=0,\end{aligned}\tag{12}$$

$$\begin{aligned}&\frac{1}{Pr}\theta''-h\theta'+Nb\left(\theta'\phi'+\gamma_3\left(h\theta'\phi''+h\theta''\phi'\right)\right)+Nt\left((\theta')^2+2\gamma_3 h\theta'\theta''\right)\\&-\gamma_3\left(h^2\theta''+hh'\theta'\right)=0,\end{aligned}\tag{13}$$

$$\phi''-Sch\phi'-\gamma_4\left(h^2\theta''+hh'\phi'\right)+\frac{Nt}{Nb}\left(\theta''+\gamma_4 h\theta'''\right)=0,\tag{14}$$

$$\chi''-Lbh\chi'-Pe\left(\chi'\phi'+\phi''(\gamma_5+\chi)\right)=0,\tag{15}$$

$$f=\Omega_1,\ g=1,\ h=0,\ \theta=1,\ \phi=1,\ \chi=1\ at\ \zeta=0,\tag{16}$$

$$f\to 0,\ g\to 0,\ h\to 0,\ \theta\to 0,\ \phi\to 0,\ \chi\to 0\ as\ \zeta\to\infty,\tag{17}$$

where ($'$) is applied for the derivative with respect to ζ. $\beta_1=\lambda_1\Omega$ and $\beta_2=\lambda_2\Omega$ are the non-dimensional relaxation and retardation time parameters, $\gamma_3=\gamma_1\Omega$ is the non-dimensional thermal relaxation time parameter, $\gamma_4=\gamma_2\Omega$ is the non-dimensional solutal relaxation time parameter, $\Omega_1=\frac{a}{\Omega}$ is the stretching parameter, $\lambda_3=\frac{\nu_f}{k\Omega}$ is the porosity parameter, $\lambda_4=\frac{k^F}{\sqrt{k}}$ is the Darcy Forchheimer parameter, $M=\frac{\sigma_f B_0^2}{\rho_f\Omega}$ is the magnetic field parameter, $Pr=\frac{\nu_f}{\alpha}$ denotes the Prandtl number, $Lb=\frac{\nu_f}{D_n}$ is the bioconvection Levis number, $Sc=\frac{\nu_f}{D_B}$ is the Schmidt number and $Pe=\frac{bW_c}{D_n}$ is the Peclet number, $\gamma_5=\frac{N_\infty}{N_w-N_\infty}$ is the microorganisms concentration difference parameter, $Nb=\frac{\tau D_B(C_w-C_\infty)}{\nu_f}$ is the Brownian motion parameter and $Nt=\frac{\tau D_T(T_w-T_\infty)}{\nu_f T_\infty}$ represents the thermophoresis parameter.

C_F (Skin friction coefficient), Nu_r (local Nusselt), Sh_r (Sherwood number) and Nn_r (local motile density number), have the definitions

$$C_F = \frac{\tau|_{z=0}}{\rho_f (r\Omega)^2}, \tag{18}$$

where

$$\tau = \sqrt{(\tau_r)^2 + (\tau_\vartheta)^2}, \tag{19}$$

exhibits the shear stress.

$$Nu_r = \frac{-rq_1}{\alpha(T_w - T_\infty)},\ Sh_r = \frac{-rq_2}{D_B(C_w - C_\infty)},\ Nn_r = \frac{-rq_3}{D_m(N_w - N_\infty)}, \tag{20}$$

where q_1, q_2 and q_3 exhibit fluxes due to heat, mass and motile microorganisms having the formulations

$$q_1 = -\alpha T_z|_{z=0},\ q_2 = -D_B C_z|_{z=0},\ q_3 = D_m N_z|_{z=0}. \tag{21}$$

Upon employing the Eqs. (9), (18) goes to simplification as

$$C_F = Re_r^{\frac{-1}{2}} \left[\left(f'(0)\right)^2 + \left(g'(0)\right)^2 \right], \tag{22}$$

where $Re_r = \frac{r^2\Omega}{\nu_f}$ exhibits the Reynolds number.

Upon employing the Eq. (9) in Eq. (20), calculations are

$$Nu_r = -Re_r^{0.5}\theta'(0),\ Sh_r = -Re_r^{0.5}\phi'(0),\ Nn_r = -Re_r^{0.5}\chi'(0). \tag{23}$$

Computational work

Under the scenerio of HAM[52], the initial approximations and auxiliary linear operators are

$$\begin{aligned} &h_0(\zeta) = 0, f_0(\zeta) = \Omega \exp(-\zeta), g_0(\zeta) = \exp(-\zeta), \theta_0(\zeta) = \exp(-\zeta), \phi_0(\zeta) = \exp(-\zeta), \\ &\chi_0(\zeta) = \exp(-\zeta), \end{aligned} \tag{24}$$

$$\boldsymbol{L}_h = h', \boldsymbol{L}_f = f'' - f, \boldsymbol{L}_g = g'' - g', \boldsymbol{L}_\theta = \theta'' - \theta, \boldsymbol{L}_\phi = \phi'' - \phi, \boldsymbol{L}_\chi = \chi'' - \chi. \tag{25}$$

The linear operators are associated with

$$\begin{aligned} \boldsymbol{L}_h\left[E_1\right] = 0,\ \boldsymbol{L}_f\left[E_2\exp(\zeta) + E_3\exp(-\zeta)\right] = 0,\ \boldsymbol{L}_g\left[E_4\exp(\zeta) + E_5\exp(-\zeta)\right] = 0, \\ \boldsymbol{L}_\theta\left[E_6\exp(\zeta) + E_7\exp(-\zeta)\right] = 0, \boldsymbol{L}_\phi\left[E_8\exp(\zeta) + E_9\exp(-\zeta)\right] = 0,\ \boldsymbol{L}_\chi\left[E_{10}\exp(\zeta) + E_{11}\exp(-\zeta)\right] = 0, \end{aligned} \tag{26}$$

where $E_i (i = 1\text{-}11)$ present the constants.

Equations of deformation for zeroth order.

Deformation equations of zeroth order are

$$(1-q)\boldsymbol{L}_h[h(\zeta,q) - h_0(\zeta)] = q\hbar_h \aleph_h[f(\zeta,q), h(\zeta,q)], \tag{27}$$

$$(1-q)\boldsymbol{L}_f[f(\zeta,q) - f_0(\zeta)] = q\hbar_f \aleph_f[f(\zeta,q), g(\zeta,q), h(\zeta,q)], \tag{28}$$

$$(1-q)\boldsymbol{L}_g[g(\zeta,q) - g_0(\zeta)] = q\hbar_g \aleph_g[f(\zeta,q), g(\zeta,q), h(\zeta,q)], \tag{29}$$

$$(1-q)\boldsymbol{L}_\theta[\theta(\zeta,q) - \theta_0(\zeta)] = q\hbar_\theta \aleph_\theta[h(\zeta,q), \theta(\zeta,q), \phi(\zeta,q)], \tag{30}$$

$$(1-q)\boldsymbol{L}_\phi[\phi(\zeta,q) - \phi_0(\zeta)] = q\hbar_\phi \aleph_\phi[h(\zeta,q), \theta(\zeta,q), \phi(\zeta,q)], \tag{31}$$

$$(1-q)\boldsymbol{L}_\chi[\chi(\zeta,q) - \chi_0(\zeta)] = q\hbar_\chi \aleph_\chi[h(\zeta,q), \chi(\zeta,q), \phi(\zeta,q)], \tag{32}$$

where q is presented as an embedding parameter and $\hbar_f, \hbar_g, \hbar_h, \hbar_\theta, \hbar_\phi$ and $\hbar_\chi$ are the non-zero auxiliary parameters. The nonlinear operators $\aleph_f, \aleph_g, \aleph_h, \aleph_\theta, \aleph_\phi$, and $\aleph_\chi$ are defined as

$$\aleph_h[f(\zeta,q), h(\zeta,q)] = 2f(\zeta,q) + \frac{\partial h(\zeta,q)}{\partial \zeta}, \tag{33}$$

$$
\begin{aligned}
\aleph_f[f(\zeta,q),g(\zeta,q),h(\zeta,q),\theta(\zeta,q)] = & -\frac{\partial^2 f(\zeta,q)}{\partial\zeta^2} + \left(f(\zeta,q)\right)^2 - \left(g(\zeta,q)\right)^2 - \frac{\partial f(\zeta,q)}{\partial\zeta}h(\zeta,q) \\
& + \beta_1\left[\left(h(\zeta,q)\right)^2\frac{\partial^2 f(\zeta,q)}{\partial\zeta^2} + 2f(\zeta,q)\frac{\partial f(\zeta,q)}{\partial\zeta}h(\zeta,q) - 2g(\zeta,q)\frac{\partial g(\zeta,q)}{\partial\zeta}h(\zeta,q)\right] \\
& + \beta_2\left[2\left(\frac{\partial f(\zeta,q)}{\partial\zeta}\right)^2 + 2\frac{\partial f(\zeta,q)}{\partial\zeta}\frac{\partial^2 h(\zeta,q)}{\partial\zeta^2} - \frac{\partial^3 f(\zeta,q)}{\partial\zeta^3}h(\zeta,q)\right] \\
& - \frac{M}{1+m^2}\left[\frac{\partial f(\zeta,q)}{\partial\zeta} - mg(\zeta,q) - 2\beta_1 h(\zeta,q)\frac{\partial f(\zeta,q)}{\partial\zeta}\right] \\
& - \lambda_3 f(\zeta,q) - \lambda_4\left(f(\zeta,q)\right)^2,
\end{aligned}
\tag{34}
$$

$$
\begin{aligned}
\aleph_g[f(\zeta,q),g(\zeta,q),h(\zeta,q)] = & 2f(\zeta,q)g(\zeta,q) + \frac{\partial g(\zeta,q)}{\partial\zeta}h(\zeta,q) - \frac{\partial^2 g(\zeta,q)}{\partial\zeta^2} \\
& + \beta_1\left[\left(h(\zeta,q)\right)^2\frac{\partial^2 g(\zeta,q)}{\partial\zeta^2} + 2f(\zeta,q)\frac{\partial g(\zeta,q)}{\partial\zeta}h(\zeta,q) + 2g(\zeta,q)\frac{\partial f(\zeta,q)}{\partial\zeta}h(\zeta,q)\right] \\
& - \beta_2\left[h(\zeta,q)\frac{\partial^3 g(\zeta,q)}{\partial\zeta^3} - 2\frac{\partial f(\zeta,q)}{\partial\zeta}\frac{\partial g(\zeta,q)}{\partial\zeta} - 2\frac{\partial^2 h(\zeta,q)}{\partial\zeta^2}\frac{\partial g(\zeta,q)}{\partial\zeta}\right] \\
& - \frac{M}{1+m^2}\left[\frac{m\partial f(\zeta,q)}{\partial\zeta} + g(\zeta,q) - 2\beta_1 h(\zeta,q)\frac{\partial g(\zeta,q)}{\partial\zeta}\right] \\
& - \lambda_3 g(\zeta,q) - \lambda_4\left(g(\zeta,q)\right)^2,
\end{aligned}
\tag{35}
$$

$$
\begin{aligned}
\aleph_\theta[f(\zeta,q),h(\zeta,q),\theta(\zeta,q),\phi(\zeta,q)] = & \frac{1}{Pr}\frac{\partial^2\theta(\zeta,q)}{\partial\zeta^2} - h(\zeta,q)\frac{\partial\theta(\zeta,q)}{\partial\zeta} \\
& + Nb\left[\frac{\partial\theta(\zeta,q)}{\partial\zeta}\frac{\partial\phi(\zeta,q)}{\partial\zeta} + \gamma_3\left(h(\zeta,q)\frac{\partial\theta(\zeta,q)}{\partial\zeta}\frac{\partial^2\phi(\zeta,q)}{\partial\zeta^2} + h(\zeta,q)\frac{\partial^2\theta(\zeta,q)}{\partial\zeta^2}\frac{\partial\phi(\zeta,q)}{\partial\zeta}\right)\right] \\
& + Nt\left[\left(\frac{\partial\theta(\zeta,q)}{\partial\zeta}\right)^2 + 2\gamma_3 h(\zeta,q)\frac{\partial\theta(\zeta,q)}{\partial\zeta}\frac{\partial^2\theta(\zeta,q)}{\partial\zeta^2}\right] \\
& - \gamma_3\left[\left(h(\zeta,q)\right)^2\frac{\partial^2\theta(\zeta,q)}{\partial\zeta^2} + h(\zeta,q)\frac{\partial h(\zeta,q)}{\partial\zeta}\frac{\partial\theta(\zeta,q)}{\partial\zeta}\right],
\end{aligned}
\tag{36}
$$

$$
\begin{aligned}
\aleph_\phi[h(\zeta,q),\theta(\zeta,q),\phi(\zeta,q)] = & \frac{\partial^2\phi(\zeta,q)}{\partial\zeta^2} - Sch(\zeta,q)\frac{\partial\phi(\zeta,q)}{\partial\zeta} \\
& - \gamma_4\left[\left(h(\zeta,q)\right)^2\frac{\partial^2\theta(\zeta,q)}{\partial\zeta^2} + h(\zeta,q)\frac{\partial h(\zeta,q)}{\partial\zeta}\frac{\partial\phi(\zeta,q)}{\partial\zeta}\right] \\
& + \frac{Nt}{Nb}\left(\frac{\partial^2\theta(\zeta,q)}{\partial\zeta^2} + \gamma_4 h(\zeta,q)\frac{\partial^3\theta(\zeta,q)}{\partial\zeta^3}\right),
\end{aligned}
\tag{37}
$$

$$
\begin{aligned}
\aleph_\chi[h(\zeta,q),\phi(\zeta,q),\chi(\zeta,q)] = & \frac{\partial^2\chi(\zeta,q)}{\partial\zeta^2} - Lbh(\zeta,q)\frac{\partial\chi(\zeta,q)}{\partial\zeta} \\
& - Pe\left[\frac{\partial\phi(\zeta,q)}{\partial\zeta}\frac{\partial\chi(\zeta,q)}{\partial\zeta} + \frac{\partial^2\phi(\zeta,q)}{\partial\zeta^2}\left(\gamma_5 + \chi(\zeta,q)\right)\right],
\end{aligned}
\tag{38}
$$

Eq. (27) retains the B.C.

$$h(0,q) = 0. \tag{39}$$

Eq. (28) retains B.C.

$$f(0,q) = \Omega_1,\ f(\infty,q) = 0. \tag{40}$$

Eq. (29) retains B.C.

$$g(0,q) = 1,\ g(\infty,q) = 0. \tag{41}$$

Eq. (30) retains B.C.

$$\theta(0,q) = 1,\ \theta(\infty,q) = 0. \tag{42}$$

Eq. (31) retains B.C.

$$\phi(0,q) = 1, \phi(\infty,q) = 0. \tag{43}$$

Eq. (32) retains B.C.

$$\chi(0,q) = 1, \chi(\infty,q) = 0. \tag{44}$$

Upon $q = 0$ and $q = 1$, Eqs. (27–32) become

$$q = 0 \Rightarrow h(\zeta, 0) = h_0(\zeta) and q = 1 \Rightarrow h(\zeta, 1) = h(\zeta), \tag{45}$$

$$q = 0 \Rightarrow f(\zeta, 0) = f_0(\zeta) and q = 1 \Rightarrow f(\zeta, 1) = f(\zeta), \tag{46}$$

$$q = 0 \Rightarrow g(\zeta, 0) = g_0(\zeta) and q = 1 \Rightarrow g(\zeta, 1) = g(\zeta), \tag{47}$$

$$q = 0 \Rightarrow \theta(\zeta, 0) = \theta_0(\zeta) and q = 1 \Rightarrow \theta(\zeta, 1) = \theta(\zeta), \tag{48}$$

$$q = 0 \Rightarrow \phi(\zeta, 0) = \phi_0(\zeta) and q = 1 \Rightarrow \phi(\zeta, 1) = \phi(\zeta), \tag{49}$$

$$q = 0 \Rightarrow \chi(\zeta, 0) = \chi_0(\zeta) and q = 1 \Rightarrow \chi(\zeta, 1) = \chi(\zeta). \tag{50}$$

Expanding $h(\zeta, q)$, $f(\zeta, q)$, $g(\zeta, q)$, $\theta(\zeta, q)$, $\phi(\zeta, q)$ and $\chi(\zeta, q)$ through Taylor series, Eqs. (45–50) generate

$$h(\zeta, q) = h_0(\zeta) + \sum_{m=1}^{\infty} h_m(\zeta) q^m, \quad h_m(\zeta) = \frac{1}{m!} \frac{\partial^m h(\zeta, q)}{\partial \zeta^m} |_{q=0}, \tag{51}$$

$$f(\zeta, q) = f_0(\zeta) + \sum_{m=1}^{\infty} f_m(\zeta) q^m, \quad f_m(\zeta) = \frac{1}{m!} \frac{\partial^m f(\zeta, q)}{\partial \zeta^m} |_{q=0}, \tag{52}$$

$$g(\zeta, q) = g_0(\zeta) + \sum_{m=1}^{\infty} g_m(\zeta) q^m, \quad g_m(\zeta) = \frac{1}{m!} \frac{\partial^m g(\zeta, q)}{\partial \zeta^m} |_{q=0}, \tag{53}$$

$$\theta(\zeta, q) = \theta_0(\zeta) + \sum_{m=1}^{\infty} \theta_m(\zeta) q^m, \quad \theta_m(\zeta) = \frac{1}{m!} \frac{\partial^m \theta(\zeta, q)}{\partial \zeta^m} |_{q=0}, \tag{54}$$

$$\phi(\zeta, q) = \phi_0(\zeta) + \sum_{m=1}^{\infty} \phi(\zeta) q^m, \quad \phi(\zeta) = \frac{1}{m!} \frac{\partial^m \phi(\zeta, q)}{\partial \zeta^m} |_{q=0}, \tag{55}$$

$$\chi(\zeta, q) = \chi_0(\zeta) + \sum_{m=1}^{\infty} \chi_m(\zeta) q^m, \quad \chi_m(\zeta) = \frac{1}{m!} \frac{\partial^m \chi(\zeta, q)}{\partial \zeta^m} |_{q=0} . \tag{56}$$

From Eqs. (51–56), the convergence of the series is obtained by taking $q = 1$ for the appropriate values of $\hbar_f$, $\hbar_g$, $\hbar_h$, $\hbar_\theta$, $\hbar_\phi$ and $\hbar_\chi$, so

$$h(\zeta) = h_0(\zeta) + \sum_{m=1}^{\infty} h_m(\zeta), \tag{57}$$

$$f(\zeta) = f_0(\zeta) + \sum_{m=1}^{\infty} f_m(\zeta), \tag{58}$$

$$g(\zeta) = g_0(\zeta) + \sum_{m=1}^{\infty} g_m(\zeta), \tag{59}$$

$$\theta(\zeta) = \theta_0(\zeta) + \sum_{m=1}^{\infty} \theta_m(\zeta), \tag{60}$$

$$\phi(\zeta) = \phi_0(\zeta) + \sum_{m=1}^{\infty} \phi(\zeta), \tag{61}$$

$$\chi(\zeta) = \chi_0(\zeta) + \sum_{m=1}^{\infty} \chi(\zeta). \tag{62}$$

Deformation equations of *m*-th order. Equations having m-th order deformations become

$$\boldsymbol{L}_h[h_m(\zeta) - \psi_m h_{m-1}(\zeta)] = \hbar_h \mathfrak{R}_m^h(\zeta), \tag{63}$$

$$\boldsymbol{L}_f[f_m(\zeta) - \psi_m f_{m-1}(\zeta)] = \hbar_f \mathfrak{R}_m^f(\zeta), \tag{64}$$

$$\boldsymbol{L}_g[g_m(\zeta) - \psi_m g_{m-1}(\zeta)] = \hbar_g \mathfrak{R}_m^g(\zeta), \tag{65}$$

$$\boldsymbol{L}_\theta[\theta_m(\zeta) - \psi_m \theta_{m-1}(\zeta)] = \hbar_\theta \mathfrak{R}_m^\theta(\zeta), \tag{66}$$

$$\boldsymbol{L}_\phi[\phi_m(\zeta) - \psi_m \phi_{m-1}(\zeta)] = \hbar_\phi \mathfrak{R}_m^\phi(\zeta), \tag{67}$$

$$\boldsymbol{L}_\chi[\chi_m(\zeta) - \psi_m \chi_{m-1}(\zeta)] = \hbar_\chi \mathfrak{R}_m^\chi(\zeta), \tag{68}$$

$$h_m(0) = 0, \tag{69}$$

$$f_m(0) = 0, f_m(\infty) = 0, \tag{70}$$

$$g_m(0) = 0, g_m(\infty) = 0, \tag{71}$$

$$\theta_m(0) = 0, \theta_m(\infty) = 0, \tag{72}$$

$$\phi_m(0) = 0, \phi_m(\infty) = 0, \tag{73}$$

$$\chi_m(0) = 0, \chi_m(\infty) = 0, \tag{74}$$

where

$$\mathfrak{R}_m^h(\zeta) = h'_{m-1} + 2f_{m-1}, \tag{75}$$

$$\begin{aligned}
\mathfrak{R}_m^f(\zeta) = & -f''_{m-1} + \sum_{k=o}^{m-1} f_{m-1-k} f_k - \sum_{k=o}^{m-1} g_{m-1-k} g_k + \sum_{k=o}^{m-1} f'_{m-1-k} h_k \\
& + \beta_1 \left[\textstyle\sum_{k=o}^{m-1} h_{m-1-k} \sum_{l=o}^{k} h_{k-l} f''_l + 2\sum_{k=o}^{m-1} f_{m-1-k} \sum_{l=o}^{k} f'_{k-l} h_l - 2\sum_{k=o}^{m-1} g_{m-1-k} \sum_{l=o}^{k} g'_{k-l} h_l \right] \\
& + \beta_2 \sum_{k=o}^{m-1} \left[2f'_{m-1-k} f_k + 2f'_{m-1-k} h''_k - f'''_{m-1-k} h_k \right] \\
& - \frac{M}{1+m^2} \left[f'_{m-1} - m g_{m-1} - 2\beta_1 \textstyle\sum_{k=o}^{m-1} h_{m-1-k} f'_k \right] \\
& \lambda_3 f_{m-1} - \lambda_4 \sum_{k=o}^{m-1} f_{m-1-k} f_k,
\end{aligned} \tag{76}$$

$$\begin{aligned}
\mathfrak{R}_m^g(\zeta) = & -g''_{m-1} + \sum_{k=o}^{m-1} g'_{m-1-k} h_k + 2\sum_{k=o}^{m-1} f_{m-1-k} g_k \\
& + \beta_1 \left[\textstyle\sum_{k=o}^{m-1} h_{m-1-k} \sum_{l=o}^{k} h_{k-l} g''_l + 2\sum_{k=o}^{m-1} f_{m-1-k} \sum_{l=o}^{k} g'_{k-l} h_l + 2\sum_{k=o}^{m-1} g_{m-1-k} \sum_{l=o}^{k} f'_{k-l} h_l \right] \\
& - \beta_2 \sum_{k=o}^{m-1} \left[h_{m-1-k} g'''_k - 2f'_{m-1-k} g'_k - 2h''_{m-1-k} g'_k \right] \\
& - \frac{M}{1+m^2} \left[m f'_{m-1} + g_{m-1} - 2\beta_1 \textstyle\sum_{k=o}^{m-1} h_{m-1-k} g'_k \right] \\
& \lambda_3 g_{m-1} - \lambda_4 \sum_{k=o}^{m-1} g_{m-1-k} g_k,
\end{aligned} \tag{77}$$

Profiles	Waqas et al.[41]	Author's computations
$f'(0)$	0.5101162642	0.5101162641
$g'(0)$	0.6158492795	0.6158492796
θ′(0)	0.933641126	0.933641125

Table 1. Data presented as the comparsion of author's computations.

$$\begin{aligned}\Re_m^{\theta}(\zeta) =&\frac{1}{Pr}\theta''_{m-1} - \sum_{k=o}^{m-1} h_{m-1-k}\theta'_k \\ &+ Nb\left[\sum_{k=o}^{m-1}\theta'_{m-1-k}\phi'_k + \gamma_3\left(\sum_{k=o}^{m-1} h_{m-1-k}\sum_{l=o}^{k}\theta'_{k-l}\phi''_l + \sum_{k=o}^{m-1} h_{m-1-k}\sum_{l=o}^{k}\theta''_{k-l}\phi'_l\right)\right] \\ &+ Nt\left[\sum_{k=o}^{m-1}\theta'_{m-1-k}\theta'_k + 2\gamma_3\sum_{k=o}^{m-1} h_{m-1-k}\sum_{l=o}^{k}\theta'_{k-l}\theta''_l\right] \\ &- \gamma_3\sum_{k=o}^{m-1} h_{m-1-k}\sum_{l=o}^{k}\left[h_{k-l}\theta''_l + h'_{k-l}\theta'_l\right],\end{aligned} \tag{78}$$

$$\begin{aligned}\Re_m^{\phi}(\zeta) =&\phi''_{m-1} - Sc\sum_{k=o}^{m-1} h_{m-1-k}\phi'_k - \gamma_4\sum_{k=o}^{m-1} h_{m-1-k}\sum_{l=o}^{k}\left[h_{k-l}\theta''_l + h'_{k-l}\phi'_l\right] \\ &+ \frac{Nt}{Nb}\left[\theta''_{m-1} + \gamma_4\sum_{k=o}^{m-1} h_{m-1-k}\theta'''_k\right],\end{aligned} \tag{79}$$

$$\Re_m^{\chi}(\zeta) =\chi''_{m-1} - Lb\sum_{k=o}^{m-1} h_{m-1-k}\chi'_k - Pe\sum_{k=o}^{m-1}\left[\chi'_{m-1-k}\phi'_k + \phi''_{m-1-k}\chi_k\right] - \gamma_5 Pe\phi''_m, \tag{80}$$

$$\psi_m =\begin{cases} 0, & m \leqslant 1 \\ 1, & m > 1.\end{cases} \tag{81}$$

For the particular solutions $h_m^*(\zeta), f_m^*(\zeta), g_m^*(\zeta), \theta_m^*(\zeta), \phi_m^*(\zeta)$ and $\chi_m^*(\zeta)$, the general evaluations of Eqs. (63–68) are

$$h_m(\zeta) =h_m^*(\zeta) + E_1, \tag{82}$$

$$f_m(\zeta) =f_m^*(\zeta) + E_2\exp(-\zeta) + E_3\exp(\zeta), \tag{83}$$

$$g_m(\zeta) =g_m^*(\zeta) + E_4\exp(-\zeta) + E_5\exp(\zeta), \tag{84}$$

$$\theta_m(\zeta) =\theta_m^*(\zeta) + E_6\exp(-\zeta) + E_7\exp(\zeta), \tag{85}$$

$$\phi_m(\zeta) =\phi_m^*(\zeta) + E_8\exp(-\zeta) + E_9\exp(\zeta), \tag{86}$$

$$\chi_m(\zeta) =\chi_m^*(\zeta) + E_{10}\exp(-\zeta) + E_{11}\exp(\zeta). \tag{87}$$

Comparsion of authors computations to existing values

Data is given in Table 1 for the authentication of authors work.

Results and discussion

In Fig. 2, β_1 shows the effect of non-dimensional relaxation time parameter on radial velocity $f(\zeta)$ which tends to decrement. As the relaxation time parameter is the ratio of material relaxation time to the material observation time. So it is physically justified that for the greater values of β_1, the high values of relaxation time address that the liquid remains solid-like in major due to which the fluid flow decreases in each side. For the effect of retardation time parameter β_2 on radial velocity $f(\zeta)$, Fig. 3 is sketched which remarks that the magnitude of flow is decelerated. Retardation time shows the time spent on the generation of shear stress in a fluid. So it presents the time-scales noted during the start-up experiments that are not interpreted through relaxation time. $\beta_1 = 0$ and $\beta_2 = 0$ correspond to the study of viscous nanofluid. Figure 4 depicts that the radial velocity $f(\zeta)$ is decelerated due to magnetic field parameter M. The interface of strong magnetic field represents remarkable decay of the flow of fluid. As M is assuming the high values, the Lorentz forces come into play which reduce the liquid flow. The existence of magnetic field challenge the flowing status and finally decelerates the radial velocity. So

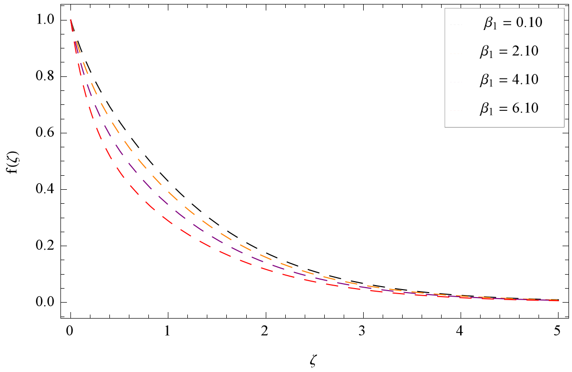

Figure 2. Pattern of graph curves on account of β_1.

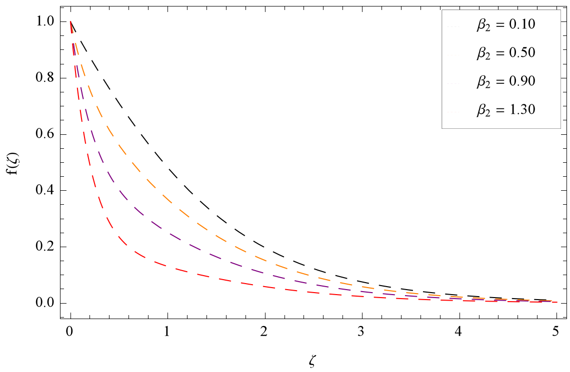

Figure 3. Pattern of graph curves on account of β_2.

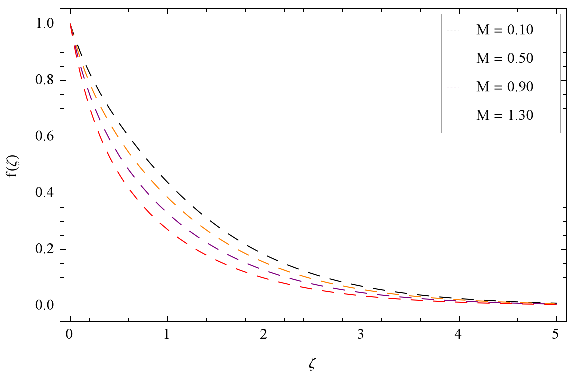

Figure 4. Pattern of graph curves on account of M.

magnetohydrodynamics is a procedure which control the fluid motion. $M = 0$, shows the absence of magnetohydrodynamic effect. Porosity parameter λ_3 enhances the flow function of fluid as shown in Fig. 5. Similarly the Darcy Forchheimer parameter λ_4 highlightes the flow of the Oldroyd-B nanofluid which is shown in Fig. 6. The stretching parameter Ω_1 effect is shown in Fig. 7. It is noted that for the greater values of the stretching parameter Ω_1, the radial velocity $f(\zeta)$ is enhanced since the stretching phenomena increases in radial direction i.e. uplifting behavior is seen for the radial velocity for the stretching values of Ω_1.

Figure 8 reports that azimuthal velocity $g(\zeta)$ has high magnitude for the non-dimensional relaxation time parameter β_1. It is noted that the flow is enhanced in the negative direction. Physically, during rotation, the disk is playing the role of centrifugal pump which pushes the fluid in the outward direction. Figure 9 displays the impact of the non-dimensional retardation time parameter β_2 on the azimuthal velocity $g(\zeta)$ which enhances for the variation of β_2 through the values 0.10, 1.10, 2.10 & 3.10. Physically, retardation time shows the time spent on designing the shear stress in the Oldroyd-B nanofluid. There exists a direct relation of retardation

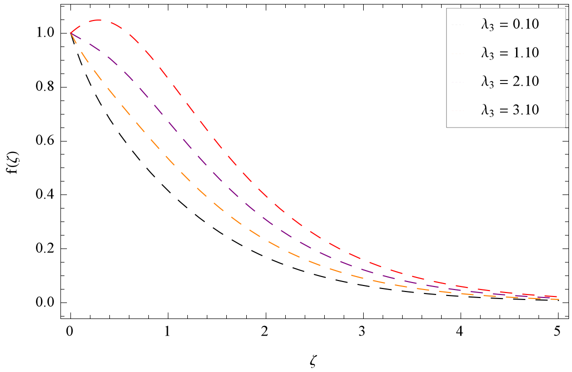

Figure 5. Pattern of graph curves on account of λ_3.

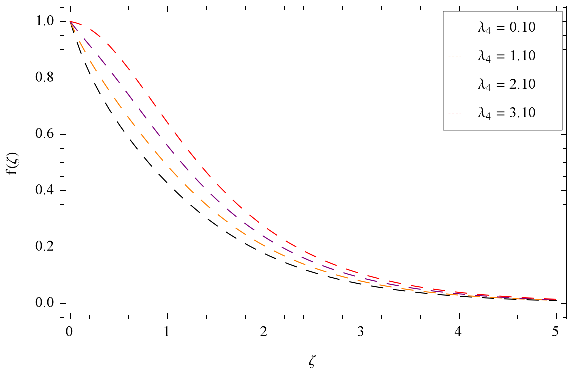

Figure 6. Pattern of graph curves on account of λ_4.

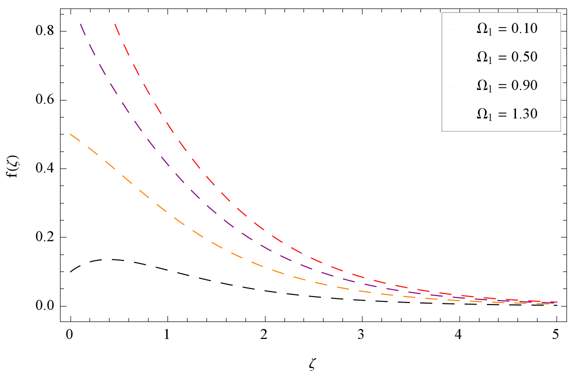

Figure 7. Pattern of graph curves on account of Ω_1.

time parameter β_2 and azimuthal velocity $g(\zeta)$. It is concluded that fluid flowing along the disk is maximum. Figures 10 and 11 remark that azimuthal velocity $g(\zeta)$ is on the high position for the various values of porosity parameter λ_3 and Darcy Forchheimer parameter λ_4 respectively. Figure 12 is drawn to understand the influence magnetohydrodynamics on azimuthal velocity $g(\zeta)$. The azimuthal velocity $g(\zeta)$ is made strong in flow due to the high external applied magnetic field.

Figure 13 depicts that the temperature is increased for the high values of Brownian motion parameter Nb. The fact is that a higher rate of Nb yields the higher diffusion. Due to Brownian motion, the extra energy is generated which in turn is used for the overshooting of temperature near the surface of rotating disk. Thermophoresis parameter Nt influence on temperature distribution $\theta(\zeta)$ is elucidated in Fig. 14. Heat transfer is decreased for larger values of Nt. The non-dimensional thermal relaxation time parameter γ_3 and temperature profile $\theta(\zeta)$ role is discussed through Fig. 15. Heat transfer is effectively enhanced via γ_3. It means that Cattaneo-Christov heat flux overcomes the heat capabality of the fluid. The scenerio is justified as when γ_3 is magnified, the Oldroyd-B

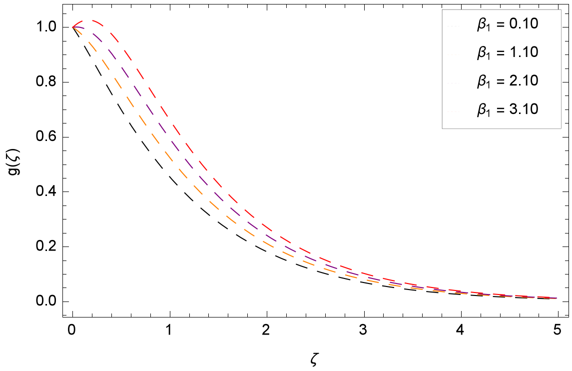

Figure 8. Pattern of graph curves on account of β_1.

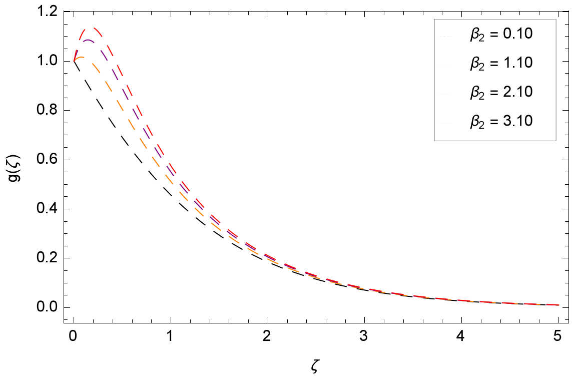

Figure 9. Pattern of graph curves on account of β_2.

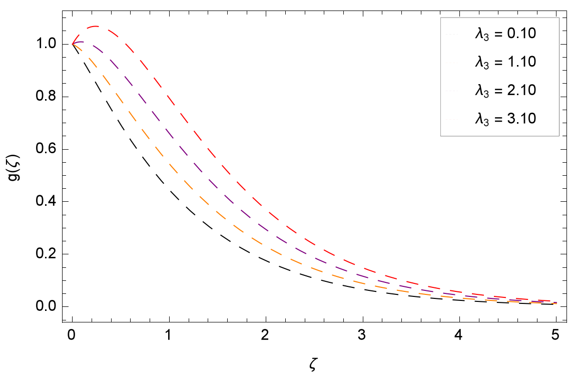

Figure 10. Pattern of graph curves on account of λ_3.

nanofluid particles transfer more heat to nearby particles and hence temerature of the sytem is made high. Supplementary heat is generated by the ineraction of nanoparticles and the base fluid due to Cattaneo-Christov heat transfer. Consequently, the thermal boundary layer is made thicker and the influence is so prominent that enhanced conduction of heat is noted in the vicinity of the disk. If $\gamma_3 = 0$, Cattaneo-Christov heat transfer model becomes the classical Fourier's law for heat transfer.

Figure 16 interpretes that nanoparticles concentration $\phi(\zeta)$ is declined with the high estimations of Schmidt number *Sc*. The reason is that the amount change in concentration across the ambient and the surface is minimum. Figure 17 reports the performances of non-dimensional solutal relaxation time parameter γ_4 and nanoparticles concentration $\phi(\zeta)$. The concentration of nanoparticles is enhanced with the high values of γ_4. The observation shows that Cattaneo-Christov mass flux has better results. Figure 18 indicates that the thermophoresis parameter *Nt* increases the nanoparticles concentration $\phi(\zeta)$ profile. Physically, the addition of *Nt* maximizes the thermal gradient in the present system due to thermophoresis in which nanoparticles move away from a

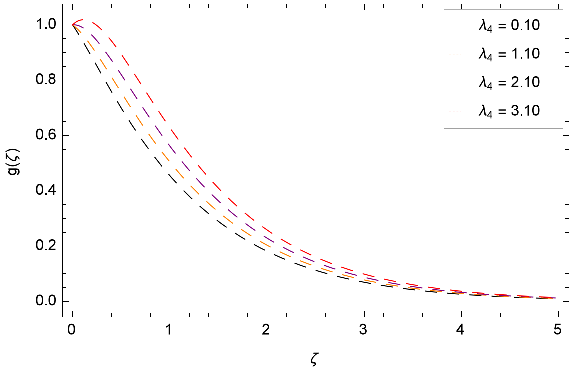

Figure 11. Pattern of graph curves on account of λ_4.

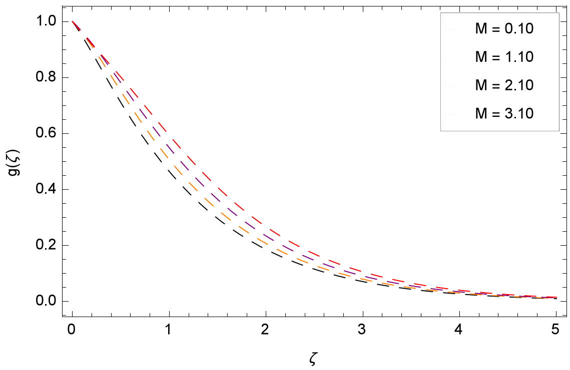

Figure 12. Pattern of graph curves on account of M.

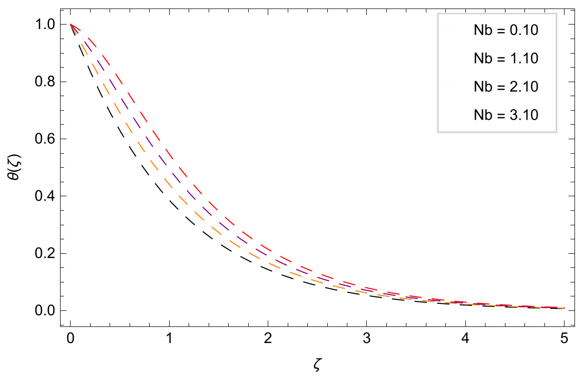

Figure 13. Pattern of graph curves on account of Nb.

higher heating location to a lower location level which increases the concentration. Due to thermophoresis an additional heat is generated by the interation nanoparticles with other particles and base fluid which intensify the nanoparticles concentration $\phi(\zeta)$. Nanoparticles concentration $\phi(\zeta)$ for the Brownian motion parameter Nb is decreased as depicted by Fig. 19. The reason is that through sufficient large values of Nb, the nanoparticles diffusion is not remarkable. In Buongiorno nanofluid model, the parameter Nb is inversely proportional to the size of nanoparticles. So with high values of Nb, smaller nanoparticles are exist which decrease the nanoparticles concentration profile $\phi(\zeta)$ due to the random motion.

The bioconvection Levis number Lb effect is shown through the Fig. 20. Bioconvection Levis number is generated on account of taking the ratio of diffusivities of momentum to mass of gyrotactic microorganisms. So due to the existence of these diffusivities, concentration $\chi(\zeta)$ of gyrotactic microorganisms is enhanced. It encourages the mixing and species diffusion in the nanofluid. Figure 21 is sketched to express the increment of gyrotactic microorganisms concentration $\chi(\zeta)$ with Peclet number Pe. The increment in gyrotactic microorganisms

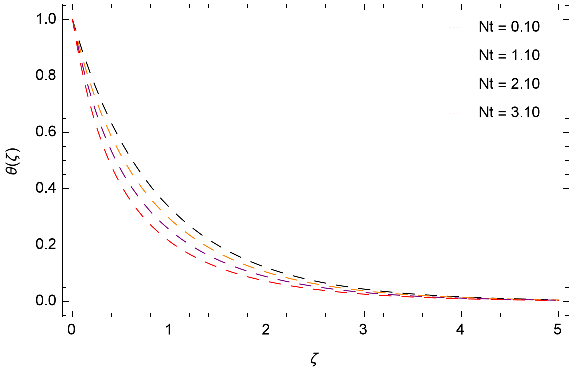

Figure 14. Pattern of graph curves on account of *Nt*.

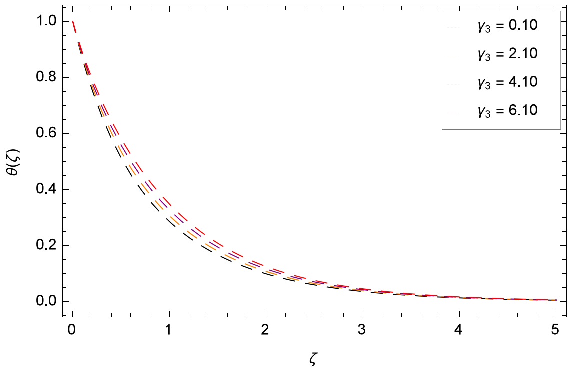

Figure 15. Pattern of graph curves on account of γ_3.

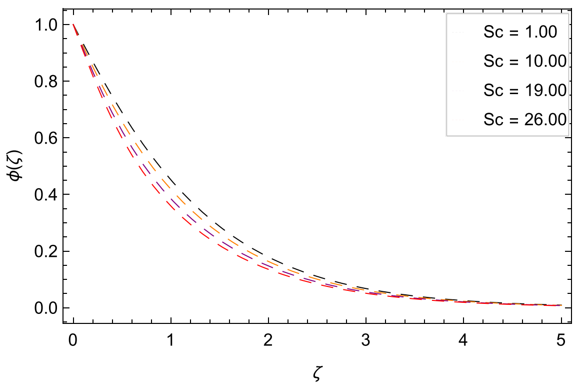

Figure 16. Pattern of graph curves on account of *Sc*.

concentration promotes the diffusion into the boundary layer of nanoparticles and gyrotactic microorganisms. Outcome of the parameter γ_5 is exhibited by Fig. 22. Favorable role uplifts the $\chi(\zeta)$. Figure 23 exhibits that *Nt* amplifies the $\chi(\zeta)$ profile. Similarly, in Fig. 24, it is exhibited that $\chi(\zeta)$ boosts with *Nb* .

Figure 25 shows that skin friction C_F is decreased with the increasing values of Hall parameter *m*. Similarly in Fig. 26, it is revealed that the Nusselt number Nu_r is a decreasing function of Brownian motion parameter *Nb*. The Sherwood number Sh_r versus Schmidt number *Sc* is shown in Fig. 27. It is observed that the Sherwood number is weakened with enhancing values of thermophoresis parameter *Nt*. On contrary to the previous cases, the motile microorganisms number Nn_r is growing large with the positive increasing values of Peclet number *Pe* as shown in Fig. 28. Tables 2, 3, 4 and 5 depict the tabulated data of skin friction coefficient, Nusselt number, Sherwood number and motile microorganisms number respectively.

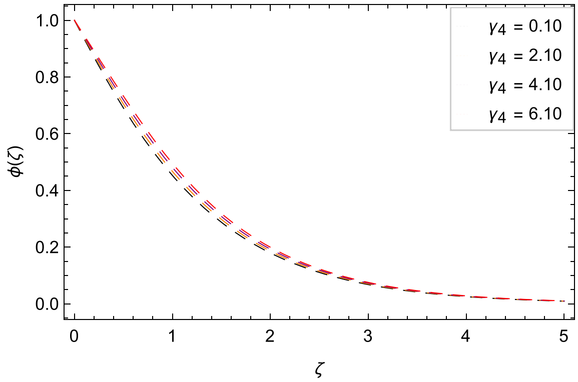

Figure 17. Pattern of graph curves on account of γ_4.

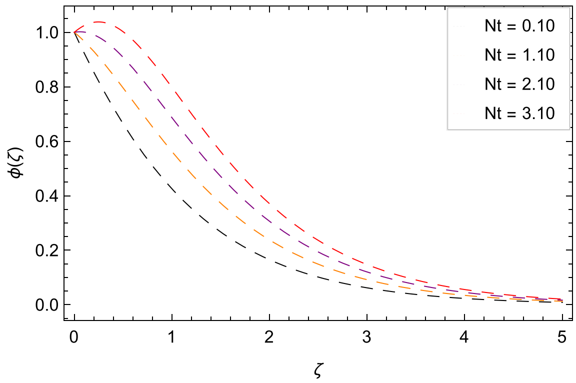

Figure 18. Pattern of graph curves on account of *Nt*.

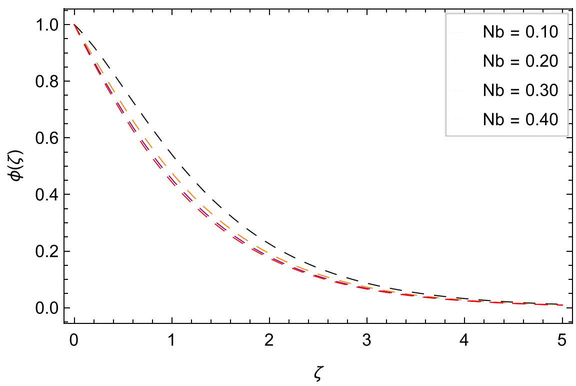

Figure 19. Pattern of graph curves on account of *Nb*.

Conclusions

The present problem can modelled in double disk with different effects which will pave the ways for further investigations.

The main results are summarised as following.

(1) The radial velocity is reduced with the increasing values of relaxation time, retardation time and magnetic field parameters while it is enhanced with porosity, Darcy Forchheimer and stretching parameters.
(2) The azimuthal velocity is enhanced with the increasing values of relaxation time, retardation time, magnetic field, porosity and Darcy Forchheimer parameters.

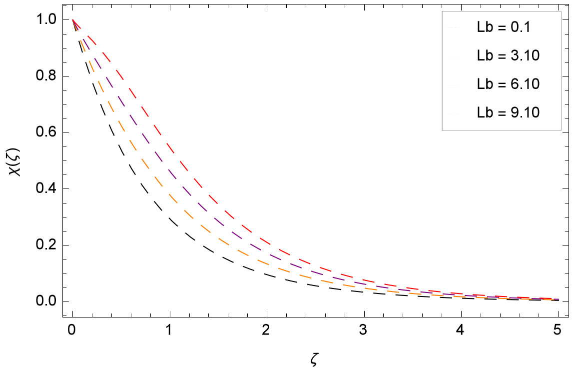

Figure 20. Pattern of graph curves on account of *Lb*.

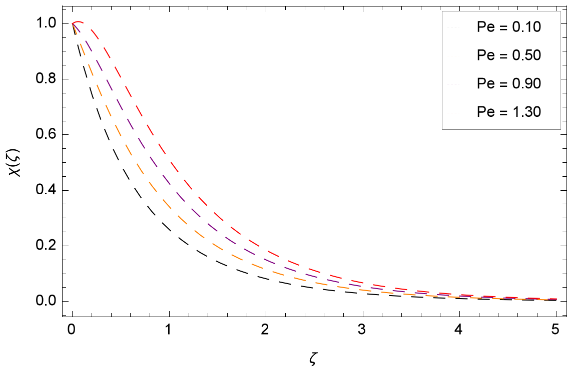

Figure 21. Pattern of graph curves on account of *Pe*.

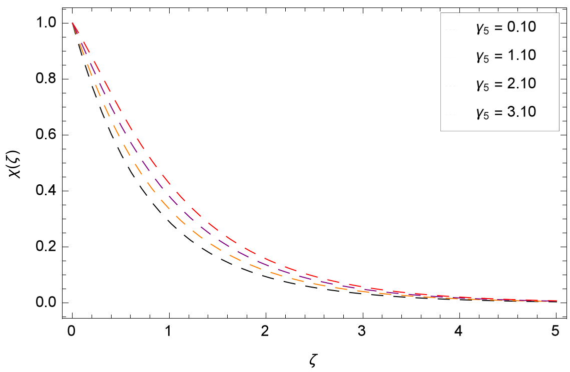

Figure 22. Pattern of graph curves on account of γ_5.

(3) The temperature is reduced with the increasing values of Brownian motion and thermophoresis parameters while it is enhanced with the thermal relaxation time parameter.
(4) The nanoparticles concentration is reduced with the increasing values of Schmidt number and thermophoresis parameter while it is enhanced with solutal relaxation time and Brownian motion parameters.
(5) The gyrotactic microorganisms concentration is enhanced with the increasing values of Peclet number, thermophoresis parameter, bioconvection Levis number, gyrotactic microorganisms concentration difference and Brownian motion parameters.
(6) The comutational work has close agreement with published material.

Data availability
Upon reasonable request to the corresponding author, the data will be provided.

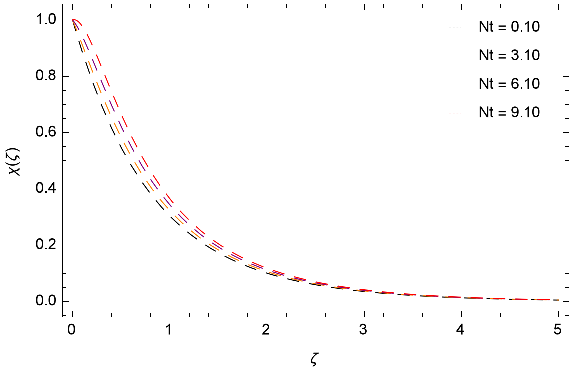

Figure 23. Pattern of graph curves on account of *Nt*.

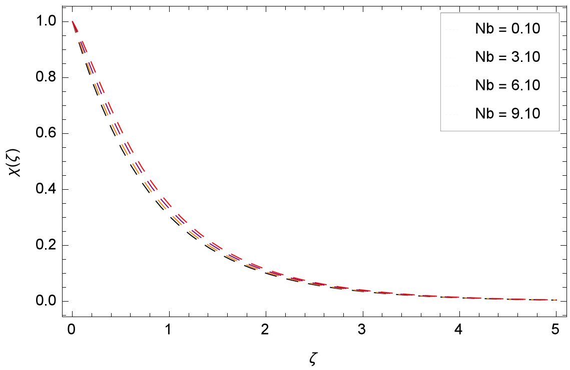

Figure 24. Pattern of graph curves on account of *Nb*.

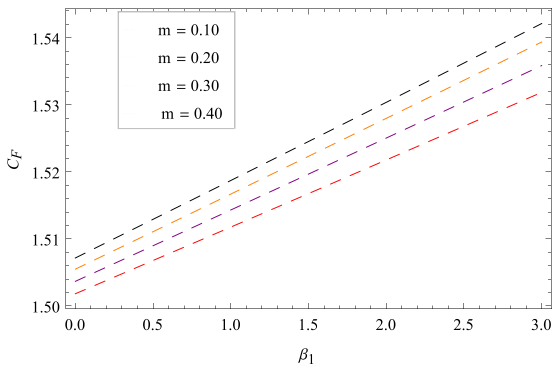

Figure 25. Pattern of graph curves on account of *m*.

Received: 5 July 2022; Accepted: 8 November 2022
Published online: 17 November 2022

References

1. Mandal, G. & Pal, D. Entropy generation analysis of radiated magnetohydrodynamic flow of carbon nanotubes nanofluids with variable conductivity and diffusivity subjected to chemical reaction. *J. Nanofluids* **10**, 491–505 (2021).
2. Yaseen, M., Rawat, S. K. & Kumar, M. Cattaneo-Christov heat flux model in Darcy-Forchheimer radiative flow of MoS_2-SiO_2/kerosene oil between two parallel rotating disks. *J. Therm. Anal. Calor.* **147**, 10865–10887 (2022).
3. Mandal, G. Convective-radiative heat transfer of Micropolar nanofluid over a vertical non-linear stretching sheet. *J. Nanofluids* **5**, 852–860 (2016).
4. Garia, R., Rawat, S. K., Kumar, M. & Yaseen, H. Hybrid nanofluid flow over two different geometries with Cattaneo-Christov heat flux model and heat generation: A model with correlation coefficient and probable error. *Chin. J. Phys.* **74**, 421–439 (2021).

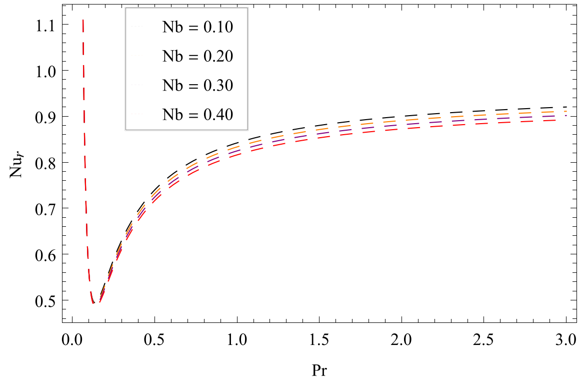

Figure 26. Pattern of graph curves on account of *Nb*.

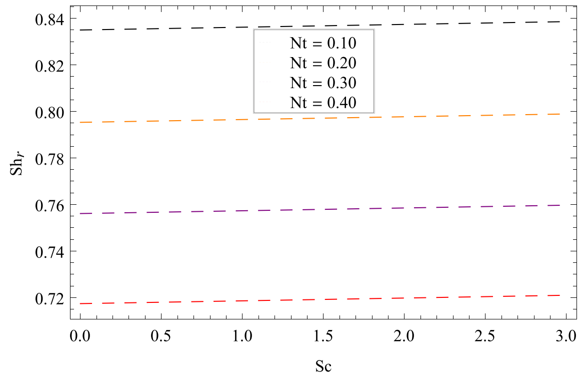

Figure 27. Pattern of graph curves on account of *Nt*.

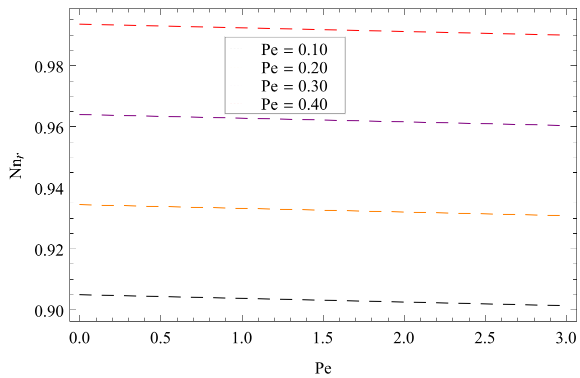

Figure 28. Pattern of graph curves on account of *Pe*.

5. Pal, D. & Mandal, G. Mixed convection-radiation on stagnation-point flow of nanofluids over a stretching/shrinkingsheet in a porous medium with heat generation and viscous dissipation. *J. Petrol. Sci. Eng.* **126**, 16–25 (2014).
6. Rawat, S. K. & Kumar, M. Cattaneo-Christov heat flux model in flow of copper water nanofluid through a stretching/shrinking sheet on stagnation point in presence of heat generation/absorption and actvation energy. *Int. J. Appl. Comp. Math.* **6**, 112 (2020).
7. Pal, D. & Mandal, G. Magnetohydrodynamic nonlinear thermal radiative heat transfer of nanofluids over a flat plat in a porous medium in existence of variable thermal conductivity and chemical reaction. *Int. J. Ambient Energy* **42**(10), 1167–1177 (2019).
8. Yaseen, M., Rawat, S. K. & Kumar, M. Hybrid nanofluid (MoS_2-SiO_2/water) flow with viscous dissipation and Ohmic heating on an irregular thick convex/concave-shaped sheet in a porous medium. *Heat Transf.* **51**, 789–10887 (2022).
9. Pal, D. & Mandal, G. Thermal radiation and MHD effects on boundary layer flow of micropolar nanofluid past a stretching sheet with non-uniform heat source/sink. *Int. J. Mech. Sci.* **126**, 308–318 (2017).
10. Pal, D. & Mandal, G. Effects of aligned magnetic field on heat transfer of water-based carbon nanotubes nanofluid over a stretching sheet with homogeneous-heterogeneous reactions. *Int. J Ambient Energy* **2**, 556 (2021).
11. Pal, D. & Mandal, G. Heat and mass transfer of a Non-Newtonian Jeffrey nanofluid over an extrusion stretching sheet with thermal radiation and nonuniform heat source/sink. *Comput. Ther. Sci. An Int. J.* **12**(2), 163–178 (2020).

m	β_1	β_2	γ_3	γ_4	Ω_1	λ_3	C_F
0.70	0.20	0.30	0.20	0.40	0.50	0.60	1.52082
1.70	–	–	–	–	–	–	1.51382
2.70	–	–	–	–	–	–	1.51478
–	1.20	–	–	–	–	–	1.54221
–	2.20	–	–	–	–	–	1.56430
–	–	1.30	–	–	–	–	1.36407
–	–	2.30	–	–	–	–	1.21920
–	–	–	1.20	–	–	–	1.21920
–	–	–	2.20	–	–	–	1.52082
–	–	–	–	1.40	–	–	1.52082
–	–	–	–	2.40	–	–	1.52082
–	–	–	–	–	1.50	–	3.37967
–	–	–	–	–	2.50	–	6.89973
–	–	–	–	–	–	1.60	1.71262
–	–	–	–	–	–	2.60	1.91410

Table 2. Numerical values of skin friction coefficient.

m	β_1	β_2	γ_3	γ_4	Ω_1	λ_3	Nu_r
0.70	0.20	0.30	0.20	0.40	0.50	0.60	0.913289
1.70	–	–	–	–	–	–	0.903289
2.70	–	–	–	–	–	–	0.912289
–	1.20	–	–	–	–	–	0.913389
–	2.20	–	–	–	–	–	0.913489
–	–	1.30	–	–	–	–	0.913589
–	–	2.30	–	–	––	–	0.913689
–	–	–	1.20	–	–	–	0.913789
–	–	–	2.20	–	–	–	0.913889
–	–	–	–	1.40	–	–	0.913989
–	–	–	–	2.40	–	–	0.913289
–	–	–	–	–	1.50	–	0.914049
–	–	–	–	–	2.50	–	0.914809
–	–	–	–	–	–	1.60	0.913289
–	–	–	–	–	–	2.60	0.913289

Table 3. Numerical values of Nusselt number.

m	β_1	β_2	γ_3	γ_4	Ω_1	λ_3	Sh_r
0.70	0.20	0.30	0.20	0.40	0.50	0.60	0.856733
1.70	–	–	–	–	–	–	0.806733
2.70	–	–	–	–	–	–	0.816733
–	1.20	–	–	–	–	–	0.826733
–	2.20	–	–	–	–	–	0.836733
–	–	1.30	–	–	–	–	0.846733
–	–	2.30	–	–	–	–	0.856733
–	–	–	1.20	–	–	–	0.866733
–	–	–	2.20	–	–	–	0.876733
–	–	–	–	1.40	–	–	0.886733
–	–	–	–	2.40	–	–	0.896733
–	–	–	–	–	1.50	–	0.856419
–	–	–	–	–	2.50	–	0.856104
–	–	–	–	–	–	1.60	0.856733
–	–	––	–	–	–	2.60	0.856733

Table 4. Numerical values of Sherwood number.

m	β_1	β_2	γ_3	γ_4	Ω_1	λ_3	Nn_r
0.70	0.20	0.30	0.20	0.40	0.50	0.60	0.981355
1.70	–	–	–	–	–	–	0.980355
2.70	–	–	–	–	–	–	0.982355
–	1.20	–	–	–	–	–	0.983355
–	2.20	–	–	–	–	–	0.984355
–	–	1.30	–	–	–	–	0.985355
–	–	2.30	–	–	–	–	0.986355
–	–	–	1.20	–	–	–	0.987355
–	–	–	2.20	–	–	–	0.988355
–	–	–	–	1.40	–	–	0.989355
–	–	–	–	2.40	–	–	0.981355
–	–	–	–	–	1.50	–	0.980355
–	–	–	–	–	2.50	–	0.980355
–	–	–	–	–	–	1.60	0.981355
–	–	–	–	–	–	2.60	0.981355

Table 5. Numerical values of motile density number.

12. Yaseen, M., Rawat, S. K. & Kumar, M. Assisting and opposing flow of a MHD hybrid nanofluid flow past a permeable moving surface with heat source/sink and thermal radiation. *Partial Diff. Eqs. Appl. Math.* **4**, 100168 (2021).
13. Gumber, P., Yaseen, M., Rawat, S. K. & Kumar, M. Heat transfer in micropolar hybrid nanofluid flow past a vertical plate in the presence of thermal radiation and suction/injection effects. *Partial Diff. Eqs. Appl. Math.* **5**, 100240 (2022).
14. Rawat, S. K., Negi, S., Upreti, H. & Kumar, M. A non-Fourier's and non-Fick's approach to study MHD mixed convective copper water nanofluid flow over flat plate subjected to convective heating and zero wall mass flux condition. *Int. J. Appl. Comput. Math.* **7**, 246 (2021).
15. Negi, S., Rawat, S. K. & Kumar, M. Cattaneo-Christov double-diffusion model with Stefan blowing effect on copper-water nanofluid flow over a stretching surface. *Heat Transf.* **50**, 5485–5515 (2021).
16. Rawat, S. K., Upreti, H. & Kumar, M. Comparative study of mixed convective MHD Cu-water nanofluid flow over a cone and wedge using modified Buongiorno's model in presence of thermal radiation and chemical reaction via Cattaneo-Christov double-diffusion model. *J. Appl. Comput. Metch.* **7**(3), 1383–1402 (2021).
17. Oldroyd, J. G. On the formulation of rheological equations of state. *Pro. R. Soc. Lond. Ser. A. Math. Phys. Sci.* **200**, 523–541 (1950).
18. Hafeez, A., Khan, M. & Ahmed, J. Thermal aspects of chemically reactive Oldroyd-B fluid flow over a rotating disk with Cattaneo-Christov heat flux theory. *J. Therm. Anal. Calor.* **144**, 793–803 (2021).
19. Shahzad, F. *et al.* Comparative numerical study of thermal features analysis between Oldroyd-B copper and molybdenum disulfide nanoparticles in engine-oil-based nanofluids flow. *Coatings* **11**, 1196 (2021).
20. Irfan, M., Khan, M., Khan, W. A., Alghamdi, M. & Ullah, M. Z. Influence of thermal-solutal stratifications and thermal aspects of non-linear radiation in stagnation point Oldroyd-B nanofluid flow. *Int. Commun. Heat Mass Transf.* **116**, 104636 (2020).
21. Anwar, T., Kumam, P., Baleanu, D., Khan, I. & Thounthong, P. Radiative heat transfer enhancement in MHD porous channel flow of an Oldroyd-B fluid under generalized boundary conditions. *Phys. Scr.* **95**, 115211 (2020).
22. Irfan, M., Aftab, R. & Khan, M. Thermal performance of Joule heating in Oldroyd-B nanomaterials considering thermal-solutal convective conditions. *Chin. J. Phys.* **71**, 444–457 (2021).
23. Khan, N. S., Shah, Q. & Sohail, A. Dynamics with Cattaneo-Christov heat and mass flux theory of bioconvection Oldroyd-B nanofluid. *Adv. Mech. Eng.* **12**(7), 1–20 (2020).
24. Irfan, M., Khan, M., Gulzar, M. M. & Khan, W. A. Chemically reactive and nonlinear radiative heat flux in mixed convection flow of Oldroyd-B nanofluid. *Appl. Nanosci.* **10**, 3133–3141 (2020).
25. Khan, M., Irfan, M., Khan, W. & Sajid, M. Consequence of convective conditions for flow of Oldroyd-B nanofluid by a stretching cylinder. *J. Braz. Soci. Mech. Sci. Eng.* **41**, 116 (2019).
26. Irfan, M., Khan, M. & Khan, W. A. Impact of non-uniform heat sink source and convective condition in radiative heat transfer to Oldroyd-B nanofluid: A revised proposed relation. *Phys. Lett. A* **383**(4), 376–382 (2019).
27. Hafeez, A., Khan, M., Ahmed, J. & Ahmed, J. Rotational flow of Oldroyd-B nanofluid subject to Cattaneo-Christov double diffusive theory. *Appl. Math. Mech. Engl. Ed.* **41**(7), 1083–1094 (2020).
28. Usman, A. H. *et al.* Computational optimization for the deposition of bioconvection thin Oldroyd-B nanofluid with entropy generation. *Sci. Rep.* **11**(1), 11641 (2021).
29. Khan, N. *et al.* Effects of homogeneous and heterogeneous chemical features on Oldroyd-B fluid flow between stretching disks with velocity and temperature boundary assumptions. *Math. Prob. Eng.* **2020**, 5284906 (2020).
30. Hashmi, M. S., Khan, N., Khan, S. U. & Rashidi, M. M. A mathematical model for mixed convective flow of chemically reactive Oldroyd-B fluid between isothermal stretching disks. *Res. Phys.* **7**, 3016–3023 (2017).
31. Tong, Z. W. *et al.* Nonlinear thermal radiation and activation energy significances in slip flow of bioconvectionof Oldroyd-B nanofluid with with Cattaneo-Christov theories. *Case Stud. Therm. Eng.* **26**, 101069 (2021).
32. Hashmi, M. S. *et al.* Dynamics of coupled reacted flow of Oldroyd-B material induced by isothermal/exothermal stretched disks with Joule heating, viscous dissipation and magnetic dipoles. *Alex. Eng. J.* **60**, 767–783 (2021).
33. Irfan, M., Khan, M. & Khan, W. A. On moel for three-dimensional Carreau fluid fow with Cattaneo-Christov double diffusion and variable conductivity: a numerical approach. *J. Braz. Soci. Mech. Sci. Eng.* **40**, 577 (2018).
34. Irfan, M., Khan, M., Muhammad, T., Waqas, M. & Khan, W. A. Analysis of energy transport considering Arrhenius activation energy and chemical reaction in radiative Maxwell nanofluid flow. *Chem. Phys. Lett.* **793**, 139323 (2022).
35. Irfan, M. Study of Brownian motion and thermophoretic diffusion on non-linear mixed convection flow of Carreau nanofluid subject to variable properties. *Surf. Interf.* **23**, 100926 (2021).
36. Khan, N. S. *et al.* Hall current and thermophoresis effects on magnetohydrodynamic mixed convective heat and mass transfer thin film flow. *J. Phys. Commun.* **3**, 035009 (2019).
37. Khan, N. S., Gul, T., Islam, S. & Khan, W. Thermophoresis and thermal radiation with heat and mass transfer in a magnetohydrodynamic thin film second-grade fluid of variable properties past a stretching sheet. *Eur. Phys. J. Plus* **132**, 11 (2017).

38. Khan, N. S. *et al.* Influence of inclined magnetic field on Carreau nanoliquid thin film flow and heat transfer with graphene nanoparticles. *Energies* **12**, 1459 (2019).
39. Waqas, H., Hussain, M., Alqarnib, M. S., Eid, M. R. & Muhammad, T. Numerical simulation for magnetic dipole in bioconvection flow of Jeffrey nanofluid with swimming motile microorganisms. *Waves Random Complex Media* **3**, 1–18 (2021).
40. Raja, M. A. Z. *et al.* Cattaneo-christov heat flux model of 3D hall current involving bioconvection nanofluidic flow with Darcy-Forchheimer law effect: Backpropagation neural networks approach. *Case Stud. Therm. Eng.* **26**, 101168 (2021).
41. Waqas, H., Imran, M., Muhammad, T., Salt, S. M. & Ellahi, R. Numerical investigation on bioconvection flow of Oldroyd-B nanofluid with non-linear thermal radiation and motile microorganisms over rotating disk. *J. Therm. Anal. Calor.* **145**, 523–539 (2021).
42. Khan, N. S. *et al.* Mechanical aspects of Maxwell nanofluid in dynamic system with irreversible analysis. *Z. Angew. Math. Mech.* **8**, e202000212 (2021).
43. Rashad, A. M. & Nabwey, H. A. Gyrotactic mixed bioconvection flow of a nanofluid past a circular cylinder with convective boundary condition. *J. Taiwan Inst. Chem. Eng.* **99**, 9–17 (2019).
44. Alwatban, A. M., Khan, S. U., Waqas, H. & Tlili, I. Interaction of Wu's slip features in bioconvection of Eyring Powell nanoparticles with activation energy. *Process* **7**, 859 (2019).
45. Lv, Y.-P., Gul, H., Ramzan, M., Chung, J. D. & Bilal, M. Bioconvection Reiner-Rivlin nanofluid flow over a rotating disk with Cattaneo-Christov flow heat flux and entropy generation analysis. *Sci. Rep.* **11**, 15859 (2021).
46. Shehzad, S. A., Reddy, M. G., Rauf, A. & Abbas, Z. Bioconvection of Maxwell nanofluid under the influence of double diffusive Cattaneo-Christov theories over isolated rotating disk. *Phys. Scr.* **2**, 66 (2019).
47. Khan, N. S., Kumam, P. & Thounthong, P. Renewable energy technology for the sustainable development of thermal system with entropy measures. *Int. J. Heat Mass Transf.* **145**, 118713 (2019).
48. Khan, N. S. Bioconvection in second grade nanofluid flow containing nanoparticles and gyrotactic microorganisms. *Braz. J. Phys.* **43**, 227–241 (2018).
49. Khan, N. S., Gul, T., Khan, M. A., Bonyah, E. & Islam, S. Mixed convection in gravity-driven thin film non-Newtonian nanofluids flow with gyrotactic microorganisms. *Result. Phys.* **7**, 4033–4049 (2017).
50. Khan, N. S. Mixed convection in MHD second grade nanofluid flow through a porous medium containing nanoparticles and gyrotactic microorganisms with chemical reaction. *Filomat* **33**, 4627–4653 (2019).
51. Khan, N. S., Shah, Z., Shutaywi, M., Kumam, P. & Thounthong, P. A comprehensive study to the assessment of Arrhenius activation energy and binary chemical reaction in swirling flow. *Sci. Rep.* **10**, 7868 (2020).
52. Shijun, L. On the homotopy analysis method for non-linear problems. *Appl. Math. Comput.* **147**, 499–513 (2004).

Acknowledgements
The authors are thankful to the respectable reviewers for their comments and suggestions. This research was supported by Research Group in Mathematics and Applied Mathematics, Department of Mathematics, Faculty of Science, Chiang Mai University. The first author is thankful to the Higher Education Commission (HEC) Pakistan for providing the technical and financial support through the Startup Research Grant Program (SRGP) under project No. 10534.

Author contributions
N.S.K., S.S., A.K., and E.T. completed the research work.

Competing interests
The authors declare no competing interests.

Additional information
Correspondence and requests for materials should be addressed to S.S.

Reprints and permissions information is available at www.nature.com/reprints.